WEP Warwick Evans Publishing

International Journal of Materials Science and Technology Studies

ISSN: 3006-7693 (Print), ISSN: 3006-3744 (Online) | Volume 3, Number 3, Year 2025
DOI: https://doi.org/10.62051/ijmsts.v3n3.04
Journal homepage: https://wepub.org/index.php/IJMSTS/index

The Mineral Composition and Hydration Behavior of Cement Clinker Under Different KH Values

Jiankai Ji, Mifeng Gou *

School of Materials Science and Engineering, Henan Polytechnic University, Jiaozuo, 454003, China

*Corresponding Author: goumifeng@163.com

ABSTRACT

This study investigates the effects of varying lime saturation factors (KH = 0.85, 0.87, 0.90, 0.92) on the mineral composition and hydration behavior of low-heat Portland cement (LHC) clinker, providing theoretical guidance for its industrial production. X-ray diffraction (XRD), scanning electron microscopy (SEM), and hydration heat tests were employed to analyze the phase composition, microstructure, and hydration characteristics of the clinker. The results indicate that as KH increases, the C_3S content rises while the C_2S content decreases, leading to a significant increase in hydration heat peak values and cumulative heat release, as well as enhanced compressive strength. When KH = 0.90, the 7-day hydration heat reaches 276.8 J/g, and the 28-day compressive strength is 43.5 MPa, meeting the GB/T 200-2017 standard for low-heat cement (≤260 J/g) while exhibiting excellent mechanical performance.

KEYWORDS

Low-Heat Portland cement; Hydration heat; Clinker mineralogy

1. INTRODUCTION

The heat release from cement hydration is an inherent phenomenon in the concrete hardening process, but its temperature rise effect is particularly pronounced in mass concrete structures. Due to the low thermal conductivity of concrete, the accumulated hydration heat in the interior is difficult to dissipate rapidly, resulting in a significant internal-external temperature difference (typically exceeding 25°C) [1], which in turn induces thermal stress. When the surface tensile stress surpasses the tensile strength of concrete, cracks develop, severely threatening structural integrity and durability [2, 3]. For example, in the Baihetan Hydropower Station dam, the internal concrete temperature can reach peak values of 50–70°C[4-7]. Without effective temperature control measures, the risk of through-cracks increases significantly[8]. Such cracks not only weaken the mechanical properties of concrete but also create pathways for moisture and aggressive agents, accelerating rebar corrosion and ultimately compromising the service life of the structure. Traditional temperature control methods, such as layered casting and embedded cooling pipes, can mitigate temperature rise but are associated with high costs and prolonged construction periods. Therefore, reducing hydration heat at the material source has become a fundamental solution, making the development and application of low-heat cement a key research focus [3, 9].

Low-Heat Portland Cement (LHC) achieves a significant reduction in hydration heat release rate and total heat generation by optimizing clinker mineral composition, featuring high C_2S and low C_3S and C_3A contents [4, 10, 11]. This makes LHC an ideal cementitious material for mass concrete applications. The key advantage of LHC lies in the slow hydration kinetics of C_2S, which, although

Content from this work may be used under the terms of CC BY-NC 4.0 licence (https://creativecommons.org/licenses/by-nc/4.0/).
Published by Warwick Evans Publishing.

leading to slower early strength development, allows for superior long-term strength compared to Ordinary Portland Cement (OPC), with compressive strength increasing by 3.4%–8.4% at 180 days [5, 6]. Microscopic studies indicate that LHC hydration produces longer C-S-H gel chains (MCL) and reduces calcium hydroxide (CH) content by 25%–28%, resulting in a denser pore structure and improved crack resistance by 11.9%–32.4% [7, 12]. In terms of standardization, various countries set the 7-day heat of hydration limit for LHC at 220–270 kJ/kg, while the Chinese standard GB/T 200–2017 imposes stricter requirements on fineness and strength [13, 14]. In engineering practice, LHC has been successfully applied in mega hydropower projects such as the Three Gorges and Baihetan dams [15]. Additionally, its performance has been further optimized by incorporating supplementary cementitious materials such as fly ash and slag. For instance, the Shantou International Convention and Exhibition Center project utilized LHC alongside the jump-form construction method, reducing the construction period by four months. From an environmental perspective, LHC production reduces energy consumption by 7.2%–15.3% and CO_2 emissions by 14.9%–15.7% compared to OPC, aligning with the green building development trend [16, 17]. Future research should focus on multi-scenario adaptability, full life-cycle performance optimization, and the synergistic effects of novel mineral admixtures to promote its broader application in underground utility corridors, deep-sea engineering, and other specialized fields [18].

In this study, cement clinker was prepared using different Lime Saturation Factor (KH) values to investigate the relationship between phase composition, microstructure, and hydration behavior under varying KH conditions, providing a fundamental basis for the industrial production of Low-Heat Portland Cement.

2. EXPERIMENTS

2.1. Materials

The analytically pure $CaCO_3$, Al_2O_3, Fe_2O_3, and SiO_2 used in this experiment, and the red mud was from Bayer red mud produced by Zhongzhou Aluminum Company Limited in Jiaozuo, Henan. The chemical composition of red mud analyzed by X-ray fluorescence (XRF) spectrometry is shown in Table 1, and the Fe_2O_3 content of the red mud was as high as 43.33 wt%. The minor and trace elements in red mud are listed in Table 2. The X-ray diffraction (XRD) pattern of red mud is shown in Fig. 1.

Table 1. Chemical compositions of red mud (wt%)

	Fe_2O_3	Al_2O_3	SiO_2	CaO	TiO_2	Na_2O	K_2O	SO_3	loss
RM	41.36	16.29	15.24	2.10	3.57	8.87	0.47	0.84	10.07

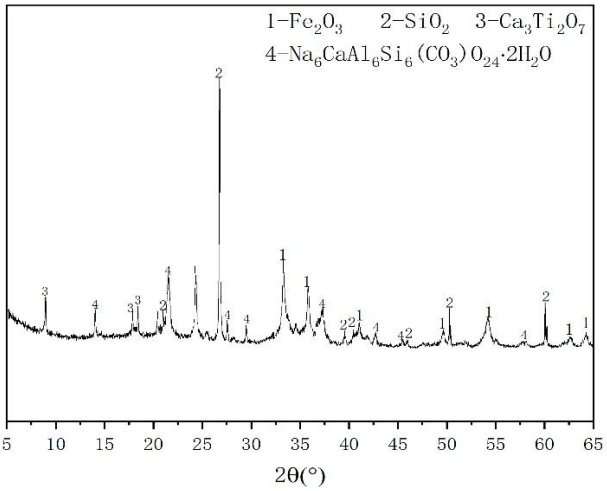

Figure 1. XRD patterns of red mud.

2.2. Preparation of the Clinker

The raw meal design with a lime saturation factor (KH) of 0.85, 0.87, 0.90, 0.92, silica ratio (SM) of 2.0, and alumina ratio (IM) of 1.0 is provided in Table 2.

Table 2. Raw materials design of clinkers (wt%)

Name	RM	Fe_2O_3	$CaCO_3$	SiO_2	Al_2O_3
K_{85}	0	3.95	77.12	3.79	15.15
K_{87}	0	3.89	77.46	3.37	14.93
K_{90}	0	3.81	77.94	3.65	14.60
K_{92}	0	3.75	78.26	3.60	14.39

Weigh the raw materials according to the raw meal proportions, mix the materials, press into tablets, calcine, cool, and sieve the powder. Then, titrate the free calcium oxide (f-CaO) content in the clinker to assess the variation in the clinker burnability with the addition of red mud. The clinker is mixed with a water-to-cement ratio of 0.5, poured into molds, and formed into 20mm×20mm×20mm cubic specimens. After demolding, the specimens are cured in water at a temperature of 20±1°C for 3, 7, and 28 days. After curing, the compressive strength is tested.

2.3. Test Methods

The free calcium oxide (f-CaO) content in the clinker is titrated using ethylene glycol as the solvent, methyl red-bromocresol green solution as the indicator, and diluted hydrochloric acid as the standard solution.

The clinker is mixed with a water-to-cement ratio of 0.5, poured into molds, and formed into 20mm×20mm×20mm cubic specimens. After demolding, the specimens are cured in water at a temperature of 20±1°C for 3, 7, and 28 days. After curing, the compressive strength at 3, 7, and 28 days is tested. The compressive strength of the clinker is measured using a pressure testing machine (YNS-Y1000, Changchun Institute of Mechanical Science and Technology), with a loading rate of 1mm/min. Six samples are tested for each group, and the average value is taken to reduce error.

The clinker is ground to pass through a 325-mesh sieve, and then the mineral phases of the clinker are analyzed using an X-ray diffraction (XRD) instrument (SmartLab, Japan). The scanning range is 10-70° 2θ, with a step size of 0.02° and a scanning speed of 5°/min. The Rietveld method is used for quantitative analysis of the mineral phases in the clinker.

The microstructure and elemental distribution of the clinker are analyzed using a scanning electron microscope (SEM) and energy dispersive spectrometer (EDS) (Merlin Compact, Carl Zeiss NTS GmbH, Germany).

The reactivity of different clinkers is measured using a thermal activity microcalorimeter (TAM AIR, TA Instruments, USA) at 20±0.2°C. For all hydration heat tests, 4.000g of clinker is mixed uniformly with 2.000g of water and placed into the calorimeter channel. The heat flow is continuously recorded for 168 hours.

3. RESULTS AND DISCUSSION

3.1. Burnability of Clinker

The variation in free lime (CaO) content in the clinker is shown in Figure 2. In all clinker samples, the free lime content remains below 1%, indicating good sintering and demonstrating the burnability of the clinker. As the Lime Saturation Factor (KH) increases, the free lime content rises from 0.36%

to 0.86%, suggesting that higher KH values make clinker calcination more challenging. However, at all KH levels, the addition of red mud significantly reduces the free lime content in the clinker[19].

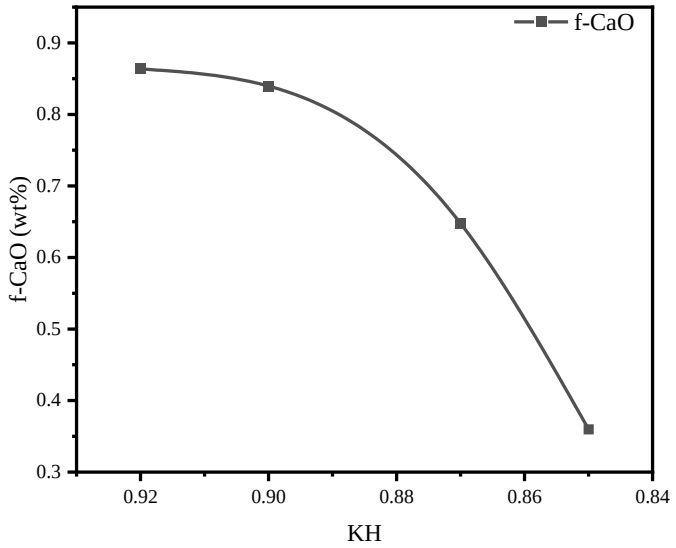

Figure 2. f-CaO content in clinker using RM instead of Fe_2O_3.

3.2. Mineralogy of Clinkers

Clinker was prepared using different Lime Saturation Factor (KH) values, and the resulting mineral composition is shown in Figure 2. It can be observed that changes in KH do not alter the primary mineral phases of the clinker, which mainly consist of C_3S, C_2S, C_4AF, and a minimal amount of C_3A. However, with increasing KH, the diffraction peak intensity of C_3S significantly increases. Given that the crystallinity of both C_3S and C_2S remains unchanged, the enhanced diffraction peak of C_3S indicates an increase in its content. This is because a higher KH provides more CaO in the clinker, which reacts with C_2S to form additional C_3S.Since C_3S contributes primarily to early strength development, the compressive strength of the clinker improves as KH increases. However, the formation of C_3S is more challenging, which explains the corresponding increase in free lime (CaO) content in the clinker with higher KH values.

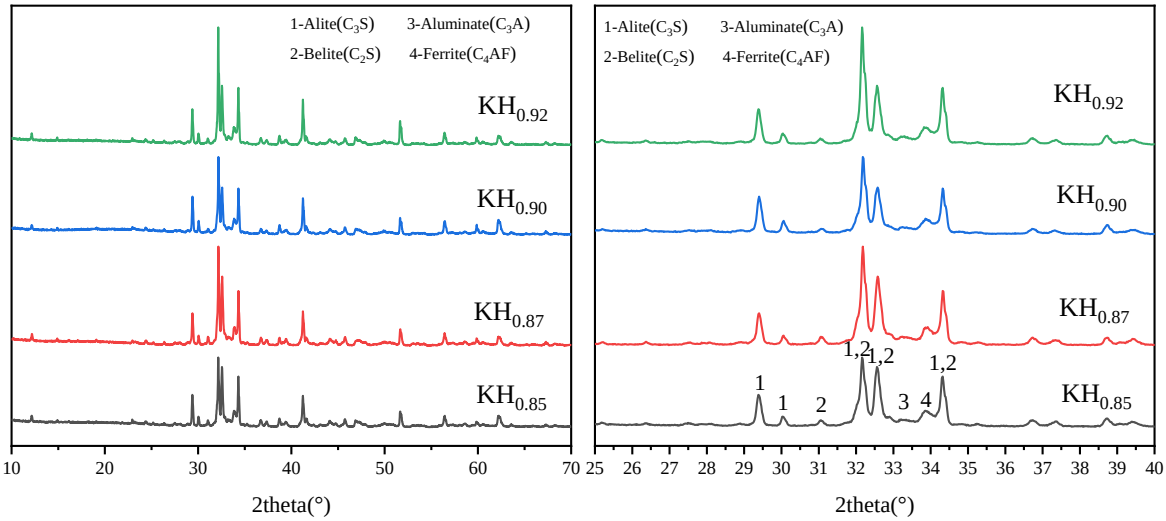

Figure 3. XRD patterns of clinker with different RM substitutions for Fe_2O_3

The clinker mineral composition, as calculated using Rietveld refinement, provides valuable insight into the relationship between the Lime Saturation Factor (KH) and the mineralogical characteristics of the clinker. Table 3 presents the detailed values, illustrating a clear trend in the mineral composition as KH increases from 0.85 to 0.92. As the Lime Saturation Factor increases, the content of C_3S rises

significantly, from 32.9% to 50.4%, while the content of C_2S decreases from 50.0% to 31.9%. This shift is primarily attributed to the increase in CaO content within the clinker. A higher KH means that more CaO is available during the clinker formation process. This excess CaO then reacts with the C_2S, facilitating the formation of more C_3S. This reaction is a key factor in explaining the observed changes in the clinker's mineral composition. Additionally, the increased content of C_3S is further validated by the enhanced intensity of its diffraction peaks in the X-ray diffraction (XRD) pattern of the clinker. The XRD results corroborate the findings from the Rietveld quantitative analysis, supporting the conclusion that the rise in KH directly influences the mineralogical phase transitions in the clinker, with a noticeable increase in C_3S and a reduction in C_2S content.

Table 3. Mineral composition of clinker calculated by Rietveld's method

	C_3S	C_4AF	C_2S	C_3A
K_{85}	32.9±1.1	50.0±1.5	14.8±0.8	2.4±0.8
K_{87}	37.9±1.3	44.7±2.2	15.1±0.9	2.3±1.1
K_{90}	47.9±1.6	34.7±1.4	15.6±0.6	2.3±0.9
K_{92}	50.4±1.9	31.9±1.1	15.6±0.9	2.1±0.7

3.3. Microstructure Analysis of Clinker

The microstructure of clinker under different Lime Saturation Factor (KH) values is shown in Figure 4; a represents the clinker with a KH of 0.85, b with a KH of 0.87, c with a KH of 0.90, and d with a KH of 0.92. None of these samples contain red mud. It can be observed that most of the clinker consists of circular crystals with sizes ranging from 5-25 μm. The morphology of these crystals is characteristic of C_2S crystals, and energy-dispersive spectroscopy (EDS) analysis shows that the Ca/Si atomic ratio is close to 2:1, confirming these crystals as C_2S. There are also some irregular prismatic-shaped crystals with sizes ranging from 10-30 μm, dispersed and surrounded by C_2S. The morphology of these crystals matches that of C_3S, and the EDS analysis shows the Ca/Si atomic ratio to be approximately 3:1, confirming these crystals as C_3S. From the micrographs of the clinker, it is evident that in similarly sized areas, the number of C_3S crystals increases as the Lime Saturation Factor (KH) rises, while the number of C_2S crystals decreases. This suggests that the C_3S/C_2S ratio in the clinker increases with higher KH. On a broader scale, this results in an increase in C_3S content and a decrease in C_2S content as the KH increases. This trend aligns with the results of X-ray quantitative analysis, which show an increase in C_3S content and a decrease in C_2S content with increasing KH. The combined results from X-ray diffraction and scanning electron microscopy further support the conclusion that as KH increases, the C_3S content rises, while the C_2S content decreases in the clinker.

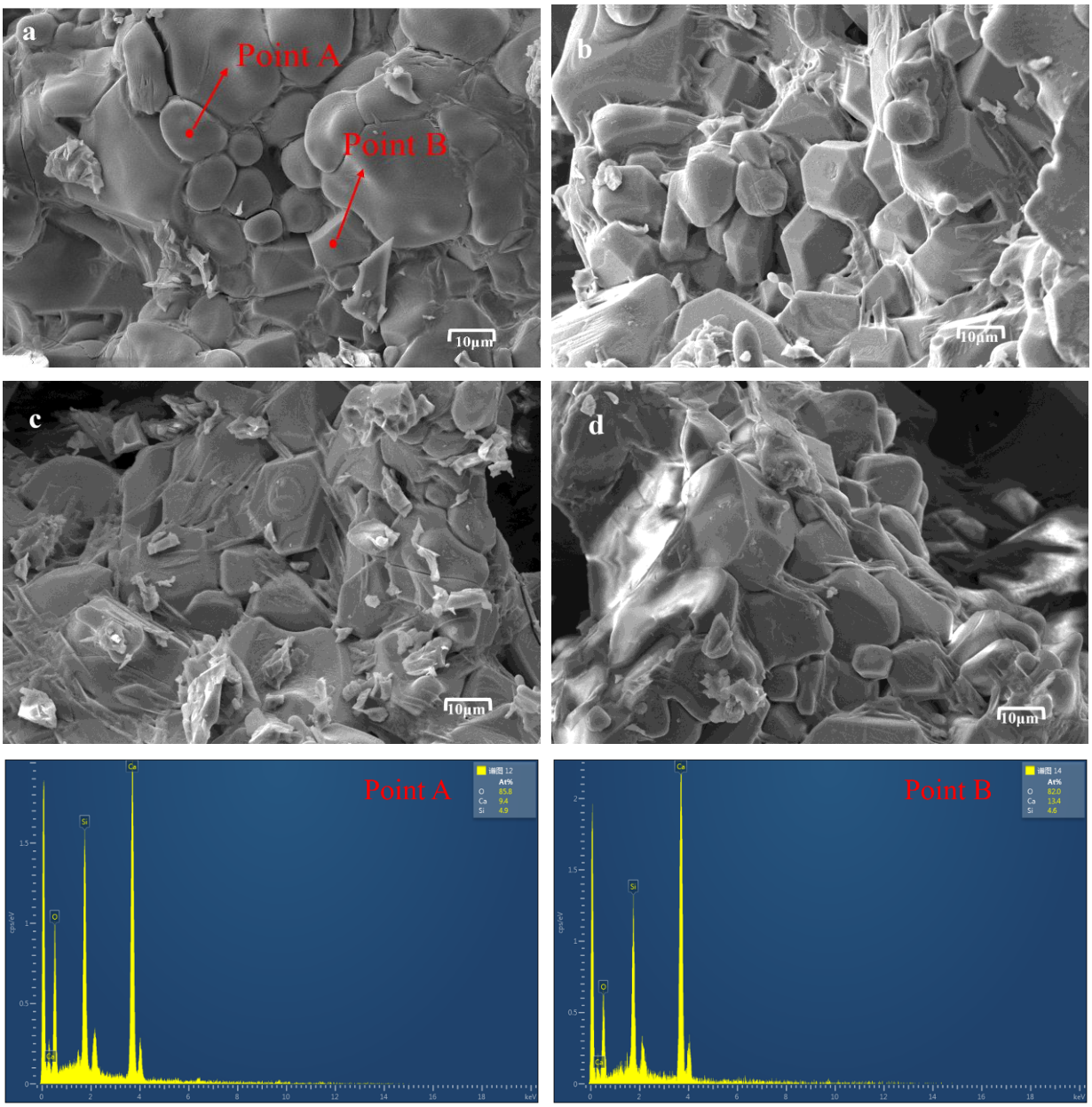

Figure 4. Microstructure of clinker with different KH; a K85, b K87, c K90, d K92

3.5. Heat of Hydration of Clinker

Figure 5 illustrates the hydration heat release rate of clinker with different KH values. As observed, the peak heat release of the cement clinker hydration reaction increases with the KH. For clinkers with a KH of 0.85, the hydration heat release peak reaches 0.86 mW/g. When the KH increases to 0.92, the peak value rises to 1.24 mW/g, making a 44% increase. With the increase in KH, only the peak value of the heat release rate is affected, while the time at which the peak occurs remains largely unchanged. This change is primarily attributed to variations in the C_3S and C_2S content in the clinker. As KH increases, the C_3S content rises significantly, while the C_2S content decreases sharply. Since C_3S releases much more heat than C_2S during hydration, this results in an overall increase in the heat release peak as the Lime Saturation Factor increases.

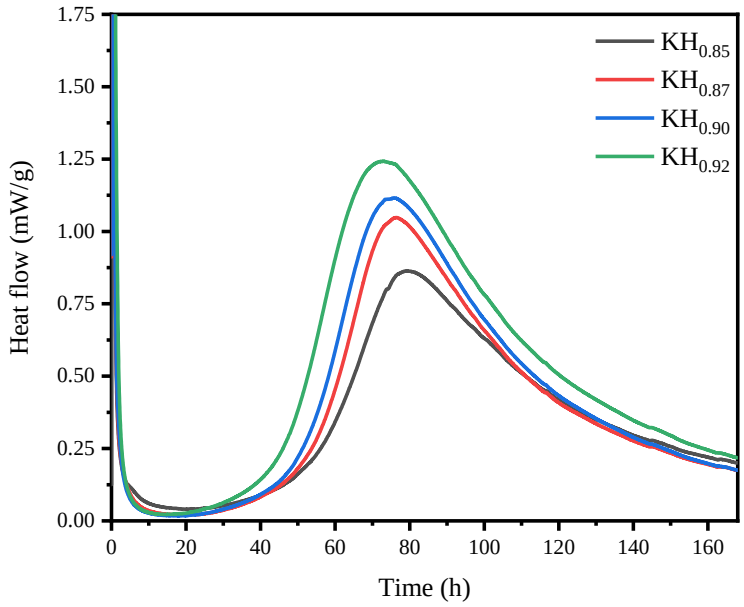

Figure 5. Heat flow of the clinker

Figure 6 presents the cumulative hydration heat release of clinker with different KH values. It is evident that the cumulative hydration heat release of cement clinker increases as KH increases. This is primarily due to the rise in C_3S content with increasing KH, as C_3S hydrates more rapidly and releases more heat compared to C_2S. From the figure, it can be observed that in the first three days, the cumulative hydration heat release of the clinker is relatively slow. When KH is 0.92, the clinker exhibits the highest cumulative heat release at three days, reaching 132.1 J/g, whereas the clinker with KH of 0.85 has the lowest cumulative heat release at 76.9 J/g. All clinker samples exhibit a three-day cumulative heat release well below the standard limits specified in GB/T 200-2017, which states that low-heat Portland cement should not exceed 230 J/g and moderate-heat Portland cement should not exceed 251 J/g within this period. However, between the third and seventh days, the hydration reaction accelerates, leading to a rapid accumulation of heat release. At seven days, the clinker with KH of 0.92 reaches a cumulative hydration heat release of 341.1 J/g, exceeding the GB/T 200-2017 standard limit of 293 J/g for moderate-heat Portland cement. The clinker with KH of 0.90 has a cumulative hydration heat release of 276.8 J/g at seven days, which is below the moderate-heat Portland cement limit but exceeds the low-heat Portland cement limit of 260 J/g. The clinkers with KH values of 0.87 and 0.85 exhibit cumulative hydration heat releases of 259.7 J/g and 242.4 J/g, respectively, both meeting the low-heat Portland cement requirement of ≤260 J/g.

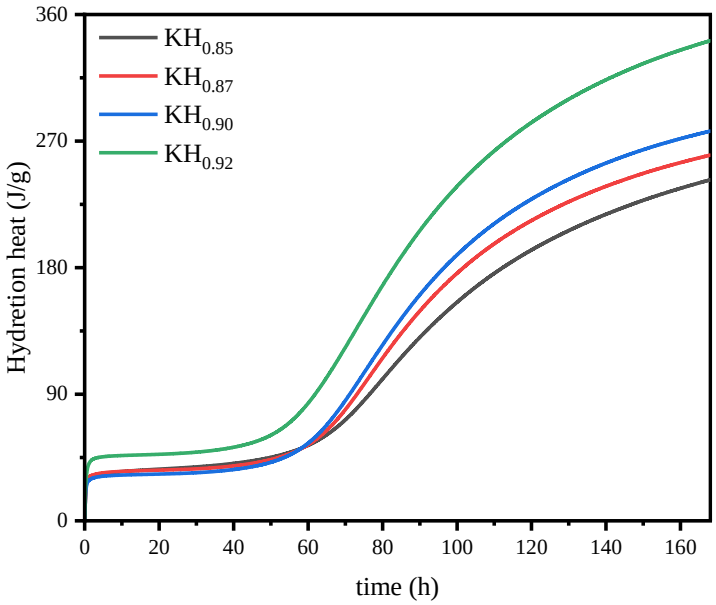

Figure 6. Cumulative heat release of clinker

3.6. Compressive Strength of Clinker

Figure 7 presents the compressive strength of clinker with different Lime Saturation Factor (KH) values. It is evident that all clinker samples exhibit relatively low compressive strength at 3 days, with the highest strength observed in K_{92} at only 8.1 MPa and the lowest in K_{85} at 3.7 MPa. This trend aligns with the thermal analysis results in Figures 5, which show that by the third day, the hydration reaction has only just begun, resulting in a limited formation of hydration products and, consequently, low compressive strength. At 7 days, a significant increase in compressive strength is observed. The lowest strength, recorded in K_{85}, reaches 14.5 MPa, whereas K_{92} achieves 30.0 MPa. After 28 days of curing, K_{85} and K_{92} exhibit compressive strengths of 32.2 MPa and 53.0 MPa, respectively. Compared to ordinary Portland cement clinker, high-iron silicate cement clinker prepared with higher SM and IM demonstrates lower early-age strength but substantial strength development at later stages. As seen in Figures 7, the compressive strength of clinker increases with higher KH values. This is primarily attributed to the rise in C_3S content, which is the main contributor to compressive strength during the hydration process. A reduction in C_3S content leads to lower compressive strength. When KH exceeds 0.90, the 7-day compressive strength of clinker surpasses 13.0 MPa, while the 28-day compressive strength exceeds 42.5 MPa, meeting the strength requirements for low-heat Portland cement as specified in GB/T 200-2017.

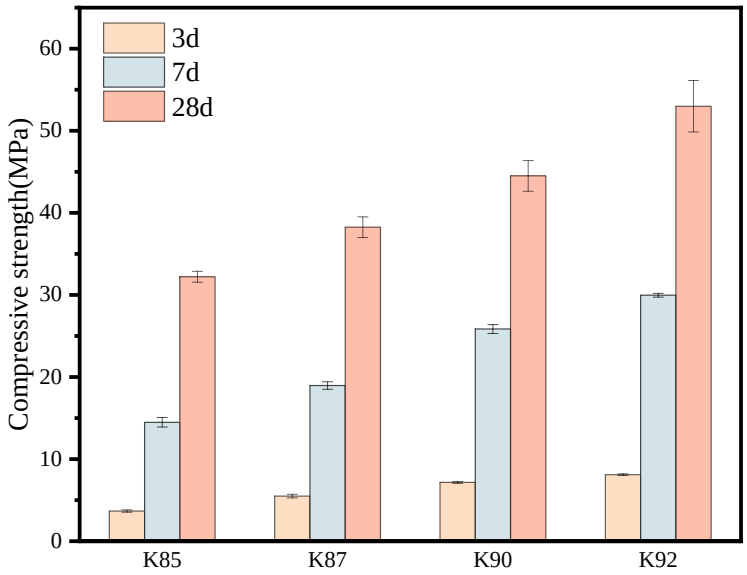

Figure 7. Compressive strength of clinker

4. CONCLUSIONS

The present study prepared cement clinkers with different Lime Saturation Factor (KH) values to investigate the variations in mineral composition and crystal structure under different KH conditions. Based on the experimental results, an optimal KH range for low-heat Portland cement clinker was determined. The main conclusions derived from the study are as follows:

(1) The f-CaO content in the clinker increases with the rise in the Lime Saturation Factor (KH), indicating that the burnability of the clinker decreases as the KH increases.

(2) The tricalcium silicate (C_3S) content in the clinker significantly increases with the rise in the Lime Saturation Factor (KH). Consequently, the hydration heat release and compressive strength of the clinker also increase accordingly.

(3) Under the conditions of SM = 2.0 and IM = 1.0, the optimal Lime Saturation Factor (KH) that meets the heat release standards for medium- and low-heat Portland cement while achieving the highest compressive strength is 0.90. At this KH value, the clinker exhibits a 3-day heat release of 92.1 J/g, a 7-day heat release of 293 J/g, and compressive strengths of 28.5 MPa at 7 days and 43.5 MPa at 28 days.

ACKNOWLEDGEMENTS

This work was financially supported by the Science and Technology Project of Henan Province (232102321145).

REFERENCES

[1] Jian S, Gao W, Lv Y, et al. Potential utilization of copper tailings in the preparation of low heat cement clinker [J]. Construction and Building Materials, 2020, 252.

[2] Ma Z, Yao Y, Liu Z, et al. Effect of calcination and cooling conditions on mineral compositions and properties of high-magnesia and low-heat Portland cement clinker [J]. Construction and Building Materials, 2020, 260.

[3] Xie J, Wu Z, Zhang X, et al. Trends and developments in low-heat portland cement and concrete: A review [J]. Construction and Building Materials, 2023, 392.

[4] Scherb S, Maier M, Köberl M, et al. Reaction kinetics during early hydration of calcined phyllosilicates in model cement systems [J]. Cement and Concrete Research, 2024, 175.

[5] Shu X, Jiang Y, Zhao Y, et al. Superimposed hydration exothermic model of cement slurry considering different reaction rates of various active substances [J]. Construction and Building Materials, 2023, 372.

[6] Yan Y, Scrivener K L, Yu C, et al. Effect of a novel starch-based temperature rise inhibitor on cement hydration and microstructure development: The second peak study [J]. Cement and Concrete Research, 2021, 141.

[7] Zhao Y, Chen P, Wang S, et al. Utilization of Bayer Red Mud Derived from Bauxite for Belite-Ferroaluminate Cement Production [J]. Journal of Renewable Materials, 2020, 8(11): 1531-41.

[8] Wang L, Dong Y, Zhou S H, et al. Energy saving benefit, mechanical performance, volume stabilities, hydration properties and products of low heat cement-based materials [J]. Energy and Buildings, 2018, 170: 157-69.

[9] Jia F, Yao Y, Wang J. Influence and Mechanism Research of Hydration Heat Inhibitor on Low-Heat Portland Cement [J]. Frontiers in Materials, 2021, 8.

[10] Yanagisawa K, Hu X, Onda A, et al. Hydration of β-dicalcium silicate at high temperatures under hydrothermal conditions [J]. Cement and Concrete Research, 2006, 36(5): 810-6.

[11] Zheng J, Wei S, Wang Q, et al. Kinetics of alite formation and ye'elimite decomposition in alite-ye'elimite cement clinker [J]. Chemical Papers, 2021, 75(11): 5983-93.

[12] Bohac M, Zezulova A, Krejci Kotlanova M, et al. Early hydration of C(4)AF with silica fume and its role on katoite composition [J]. J Microsc, 2024, 294(2): 168-76.

[13] Huang X, Hu S, Wang F, et al. The effect of supplementary cementitious materials on the permeability of chloride in steam cured high-ferrite Portland cement concrete [J]. Construction and Building Materials, 2019, 197: 99-106.

[14] Huo B, Zhang Y. Effects of dicalcium ferrite on hydration and microstructure of cementitious material [J]. Construction And Building Materials, 2024, 411.

[15] Maddalena R, Roberts J J, Hamilton A. Can Portland cement be replaced by low-carbon alternative materials? A study on the thermal properties and carbon emissions of innovative cements [J]. Journal of Cleaner Production, 2018, 186: 933-42.

[16] Wang Q, Yan P, Han S. The influence of steel slag on the hydration of cement during the hydration process of complex binder [J]. Science China-Technological Sciences, 2011, 54(2): 388-94.

[17] Xue J, Liu S, Ma X, et al. Effect of different gypsum dosage on the chloride binding properties of C4AF hydrated paste [J]. Construction and Building Materials, 2022, 315.

[18] Zhang K, Wang C, Huang X. Insight into discrepancies in hydration reactivity of ferrite phase in Portland cement clinker and synthetics [J]. Construction and Building Materials, 2024, 412.

[19] Wang K, Liu Y, Dou Z, et al. A Novel Method of Extracting Iron from High-Iron Red Mud and Preparing Low-Carbon Cement Clinker from Tailings [J]. Jom, 2022, 74(7): 2750-9.